Journal of Batteries
for Renewable Energy and Electric Vehicles (JBREV)

Journal homepage: https://journal.n-bri.org/

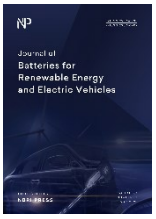

The Effect of Calcination Temperature on $LiNi_{1/3}Mn_{1/3}Co_{1/3}O_2$ Cathode Material for Lithium-Ion Batteries

S. Rahayu[1*], A. U. Saudi[2], R. Tasomara[2], M. D. Gumelar[1], W. T. Utami[2], A. U. Hapsari[2], J. Raharjo[2], S. Husin[1], D. A. Saputra[1], H. Yuliani[1], G. Taqwatomo[1], Y. A. Andrameda[2], O. P. Arjasa[1], A. Agustanhakri[1], A. H. Budiman[1]

[1]*Center for Conversion and Conservation Energy, National Research and Innovation Agency, KST BJ Habibie, Tangerang Selatan 15314, Indonesia*
[2]*Center for Advanced Materials, National Research and Innovation Agency, KST BJ Habibie, Tangerang Selatan 15314, Indonesia*

ARTICLE INFO

Article history:
Received date 23 September 2023
Received in revised form 30 September 2023
Accepted 14 October 2023

Keywords:
LIBs
NMC111
Coprecipitation
XRD
Cation mixing

ABSTRACT

The lithium-ion battery has gained popularity among other secondary batteries for portable electronic devices and electric vehicle applications, especially the $LiNi_{1/3}Co_{1/3}Mn_{1/3}O_2$ or NMC111, considering its well-balanced configuration resulting in stable and safe electrochemical performance. NMC111 has been successfully prepared using a coprecipitation process at calcination temperatures from 800 to 950°C. The physical characteristics were investigated using X-Ray Diffraction (XRD), Scanning Electron Microscopy-Energy Dispersive Spectroscopy (SEM-EDS), and Particle Size Analysis (PSA). The XRD patterns showed the rhombohedral single phase for all calcination temperatures. Meanwhile, higher calcination temperatures offer higher degree of crystallinity, lower intensity ratio and more undesirable cation mixing. The particles with a uniform rectangle or pyramid shape are observed at the calcination temperature range from 800 to 900°C. However, bigger submicron particles with a rectangle or pyramid shape are detected at a higher temperature (950°C). The SEM-EDS mapping shows the homogeneity composition for all variation calcination temperatures. PSA analysis showed that calcination temperature at 800 and 850°C gives the particle less than 400 nm suggesting a potential material for a cathode of lithium-ion batteries.

INTRODUCTION

Lithium-ion batteries (LIBs) have become the most marketable rechargeable batteries compared to its predecessors, nickel-cadmium (Ni-Cd) and nickel-metal hydride (Ni-MH), due to its transcendency in volumetric and gravimetric capacity, charge-discharge feature, and nominal voltage. Following its exceptional properties, LIBs are extensively used in wide-ranging applications, from portable electronic devices to stationary energy storage. LIBs are also the most promising technology to be utilized in the rising of electric vehicles (EVs) [1-3].

LIBs can have several chemical configurations in the cathode, such as, lithium iron phosphate (LFP), lithium cobalt oxide (LCO), lithium manganese oxide (LMO), lithium nickel manganese cobalt oxide (NMC), and lithium nickel cobalt aluminum oxide (NCA), which can directly result to the battery properties. LFP has a long cycle life and high current rating, however it has low nominal voltage and energy density.

LCO offers the highest energy density compared to other types of conventional LIBs, yet cobalt has environmental and political issues, causing the novel technology to limit the cobalt usage in cathode production [4, 5]. Meanwhile, NMC promotes great balance performance in the terms of energy, power, and thermal stability, due to the presence of nickel and manganese in the cathode along with cobalt, making NMC favorable to be used in broad application [6].

* Corresponding author.
E-mail address: srir008@brin.go.id
DOI: 10.59046/jbrev.v1i02.22

The stoichiometry of NMC can be customized to the desired needs, completing the formula of $LiNi_xMn_yCo_{1-x-y}O_2$. Each element contributes to the properties of LIBs, as nickel maintains the specific energy yet having poor stability, while manganese supports the structural and thermal stability but low specific capacity. On the other hand, cobalt as a nonmagnetic element, restricts the cation mixing phenomenon between nickel and lithium, building a strong and stable synergy in cathode material [7].

Being the most balanced configuration, $LiNi_{1/3}Co_{1/3}Mn_{1/3}O_2$, or NMC111, provides the most stable cycling performance compared to other types of NMC [2]. Although recent studies have started to synthesize nickel-rich NMC with less than 1 percent cobalt, it would be a very challenging synthesis process due to the attraction of nickel to lithium in the crystal lattice, causing the lattice collapse and structural failure of the cathode materials [8, 9]. The presence of cobalt is essential to maintain the overall battery performance, making NMC111 the most commonly used NMC battery in various applications [2].

NMC can be synthesized through several techniques, including hydrothermal, solid state, sol-gel, solvothermal, coprecipitation, combustion, spray pyrolysis, and emulsion drying. Coprecipitation is the most common process that is typically used for manufacturing NMC batteries, considering its simplicity, straightforward scalability, and economical value, compared to other synthesis methods [7].

The fundamental concept of coprecipitation is to combine the metals in stoichiometry calculation to formulate the desired precursors and coprecipitate these metals under a controlled environment [10]. For LIBs fabrication, the coprecipitated metals are ground to finer size and mixed together with lithium source, such as lithium carbonate (Li_2CO_3) or lithium hydroxide (LiOH). Lithium is added after coprecipitation process due to its lightweightness, making it easy to cease when it is blended at the initial stage. The mixture of lithium and coprecipitation metals are then sintered to acquire the active materials for cathode of LIBs [7].

The method chosen for synthesizing NMC can directly influence both physical and electrochemical characteristics of cathode materials, such as the particle size and distribution, tap density, as well as the charge/discharge capacity, cyclability, and capacity retention. Small size particles, can produce cathode materials with high surface to volume ratio, which can accommodate bigger access for lithium-ion exchange on the cathode surface and shorter path length for electron transport, which lead to improvement of charge/discharge rate and longer cycle-life [11-13].

In this study, the effect of calcination temperatures in the synthesis of cathode materials for Li-NMC battery using coprecipitation approach was investigated. The cathode powder was subjected to various tests, including X-Ray Diffraction (XRD), Particle Size Analysis (PSA), and Scanning Electron Microscopy-Energy Dispersive Spectroscopy (SEM-EDS), to analyze its physical properties, such as its particle size, density, crystalline structure, thermal stability, and morphology.

METHODOLOGY

Lithium carbonate (Li_2CO_3), sodium hydroxide (NaOH), and ammonium hydroxide (NH_3H_2O) were purchased from Merck Company. The cobalt sulfate heptahydrate ($CoSO_4.7H_2O$) used as precursor is analytical grade reactants from China. The nickel sulfate hexahydrate ($NiSO_4.6H_2O$) and manganese sulfate monohydrate ($MnSO_4.H_2O$) were technical grade precursors. Those raw materials were used to prepare the $LiNi_{1/3}Co_{1/3}Mn_{1/3}O_2$.

The $LiNi_{1/3}Co_{1/3}Mn_{1/3}O_2$ was synthesized by a coprecipitation process, followed by solid-state calcination. The details of experiment can be summarized as follows: a transition metal ion solution containing 0.67 M of $NiSO_4.6H_2O$, 0.67 M of $CoSO_4.6H_2O$, and 0.67 M of $MnSO_4.6H_2O$ was added dropwise by 4 M NaOH and 0.8 M NH_4OH in continuous stirring container. The hydroxide solution was continuously added into a container to stabilize the reaction until pH 12. The coprecipitation reaction was conducted at constant stirring speed and at steady temperature about 50°C. Then, the solution was aged for 2 hours.

Afterwards, the brownish precipitates were collected using vacuum pump filtration apparatus and washed by hot water to remove residual sodium and sulphate. Finally, the hydroxide of nickel, manganese, and cobalt precipitates were dried at 100°C overnight under vacuum. To obtain $LiNi_{1/3}Co_{1/3}Mn_{1/3}O_2$ materials, the hydroxide of nickel, manganese, and cobalt precursors were mixed with 3 wt% excess of Li_2CO_3 and calcined in air at temperature of 800, 850, 900, 950°C for 12 hours. The heating rate was maintained at 5°C/minute.

The crystal structures of materials were analyzed by powder XRD (PANalytical Aeris X-ray Diffractometer) with Cu-Kα irradiation (λ=1.5405980 Angstrom). XRD patterns were acquired in the diffraction angle (2θ) range of 10°-80° at step scan of 0.054°. Rietveld analysis of XRD patterns was performed by X'pert HighScore program. Morphological features and elemental mapping were observed by Scanning Electron Microscope-Energy Dispersive Spectroscopy (SEM-EDS) (Hitachi SU3500). Particle size distributions were determined from SEM image analysis using ImageJ program. In order to further the analysis, the particle size

distributions were obtained on powders dispersed in demineralized with Particle Size Analyzer (PSA) (Cilas Nano DS). 0.1% by weight aqueous solution of sodium hexametaphosphate was used as a dispersion medium in the measurement and the measurement was made after a 5-minute ultrasonic dispersion treatment.

RESULTS AND DISCUSSION

The XRD results for NCM111 calcined at different temperatures ranging from 800 °C to 950°C at typical duration of 12 hours are presented at Fig. 1. Using the X'pert HighScore software, the XRD pattern can be indexed in the rhombohedral with space group $R\bar{3}m$, without any impurity phase. These XRD peaks matched with the International Centre for Diffraction Data (ICDD) reference for NMC111 (4002443) [14].

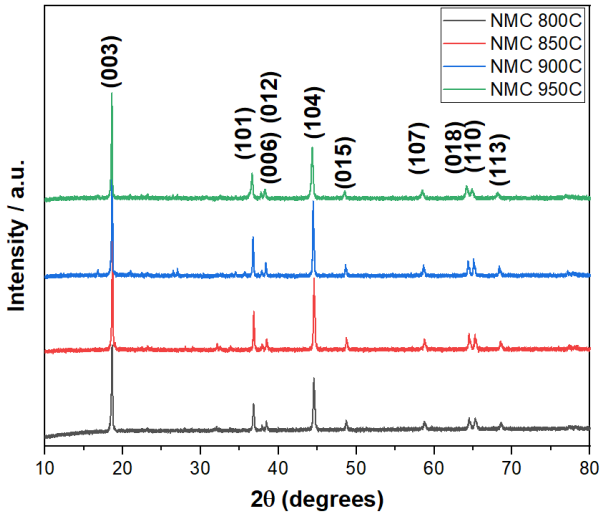

Fig. 1. XRD patterns from NMC111 samples with different calcination temperatures.

The XRD peaks at (006)/(012) and (018)/(110) (Fig. 2.) showed the clear splitting indicating the materials are well-ordered and layered hexagonal structure [15,16].

While the XRD peaks at (003) (Fig. 3.) shows the decreasing of full width at half maximum (FWHM) and higher degree of crystallinity along with the increasing calcination temperatures [14,15].

The refinement of NMC111 calcined at 800°C shown at Fig. 4. and the detailed crystallographic data from Rietveld refinements of NMC111 cathodes calcined at different temperatures summarized at Table 1. The refinement shows the good fit between the observed and the calculated patterns and indicated with the GoF values that are lower than 2. Using the Scherrer equation, the crystallite size of the material is calculated. Increasing calcination temperatures shows the growth of crystallite sizes, from 100.6 nm at temperature 800°C to 166.5 nm at 950°C.

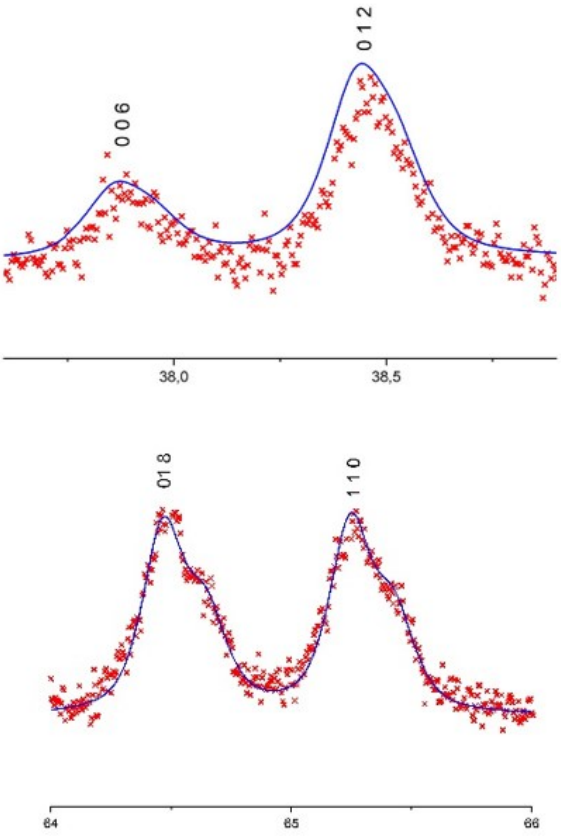

Fig. 2. Magnified view of splitting XRD peaks at (006)/(012) and (018)/(110).

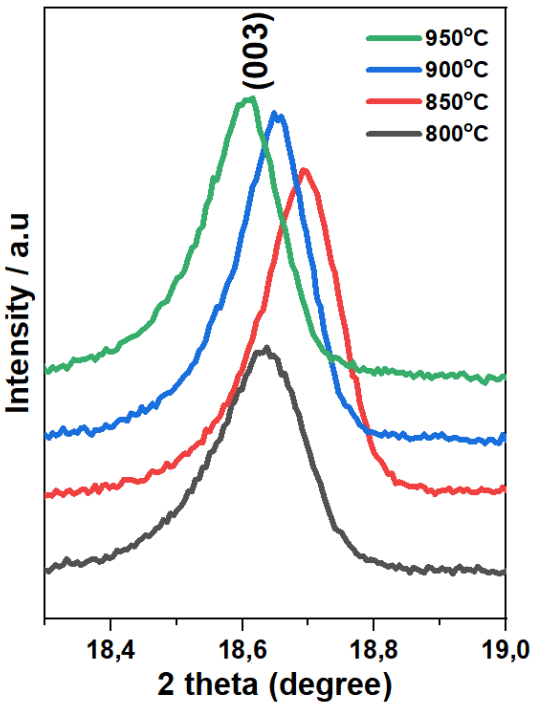

Fig. 3. Magnified view (003) and (104) XRD peaks.

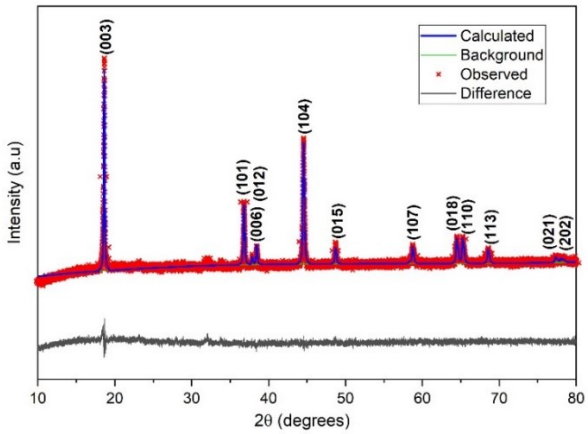

Fig. 4. Refinement profile using High-score software for NMC 111 800°C.

The cationic distribution in the α-NaFeO2-type lattice determined from the integrated intensity ratio of (003) to (104) peaks, I_{003}/I_{104}, the smaller the ratio is, the higher structural deviation from hexagonal to cubic symmetry [15]. We observe that the higher calcination temperature will decrease the intensity ratio, I_{003}/I_{104}. Calcination temperatures between 800°C and 850°C have an intensity ratio higher than 1.2, which means there is no undesirable Li/Ni cationic mixing in the structure [15-17]. However, higher calcination temperature shows an intensity ratio lower than 1.2 and creates more undesirable Li/Ni cation mixing due to the formation of slightly higher content of Ni^{3+} effect of increasing oxygen vacancies at high calcination temperature [15-17].

Table 1. Crystallographic data from Refinement data of XRD patterns for NMC111 at different calcination temperatures.

Parameters	800 °C	850 °C	900 °C	950 °C
a-axis (Å)	2.853	2.857	2.863	2.873
c-axis (Å)	14.204	14.218	14.236	14.266
c/a	4.979	4.977	4.973	4.966
Crystallite size (nm)	100.6	171.5	189.2	166.5
$I_{(003)}/I_{(104)}$	1.396	1.259	1.144	1.114
R_{exp}	2.174	2.030	2.085	2.043
R_{prof}	1.994	1.637	1.733	1.652
R_{wp}	2.656	2.261	2.434	2.219
GoF	1.492	1.241	1.362	1.181

SEM was used to analyze the particle morphology and size of NMC111 cathodes in various calcination temperatures. The uniform distribution of the rectangle or pyramid-shaped aggregates particles is observed. The particle size in NMC samples is critical in determining the high-rate-capacity, as the particle size should be below 3µm [18,19]. Similar to the research by Zheng et al., the small primary particle in NMC cathodes might enhance the high-power performance due to a higher surface area that allows more rapid interaction of lithium [20]. Figure 5a shows NMC111 calcinated at 800 °C.

The submicron particles in the size range from 150 to 450 nm, with an average of 300 nm, are observed (Fig. 5b). The nanoparticles distribution is calculated using ImageJ (100 particle measurements per sample), shown in Fig. 5b. The submicron particles also observed at NMC111 calcinated at 850 and 900 °C (Fig. 5d and 5f), ranging from 250 to 500 nm, with an average of 350 nm, and 400 to 1000 nm, with an average of 600 nm, respectively. The distribution of particles is shown in Fig. 6d and 6f. However, at temperature 950 °C (Fig. 6g), the particle size is getting bigger (micron particles) yet still below 3µm.

EDS analysis was carried out to determine the concentration and stoichiometric ratio of the cathode powder. From Table 2, it can be seen that the concentration of each calcination temperature variation is fairly similar in terms of Ni:Mn:Co ratio, which is around 1:1:1. One minor aberration is on the Mn content on the temperature of 850 °C, which shows a higher ratio compared to other samples, with the value of 1.19. From the EDS results, temperature variation of 950 °C indicates the most homogeneous Ni:Mn:Co ratio.

Table 2. EDS analysis of NMC111 at different calcination temperatures.

element	800 °C		850 °C		900 °C		950 °C	
	%wt	Ratio	%wt	Ratio	%wt	Ratio	%wt	Ratio
Ni	34.97	1.07	34.26	1.01	36.16	1.09	33.48	1.00
Mn	30.46	1.00	31.79	1.19	30.98	1.01	31.47	1.00
Co	34.57	1.06	33.95	1.00	32.86	1.00	35.05	1.04

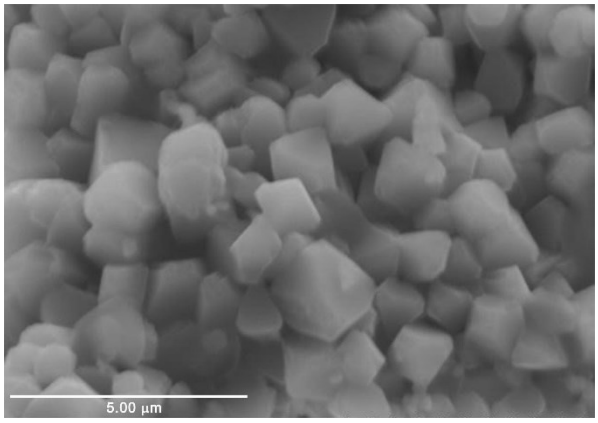

(a)

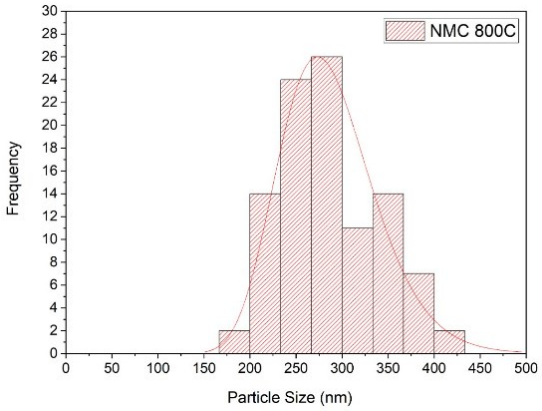

(b)

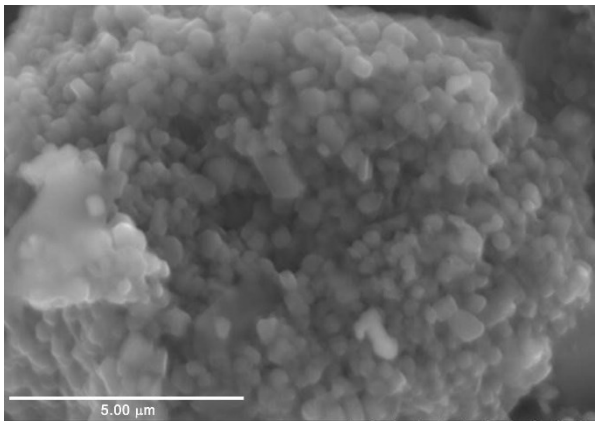

(c)

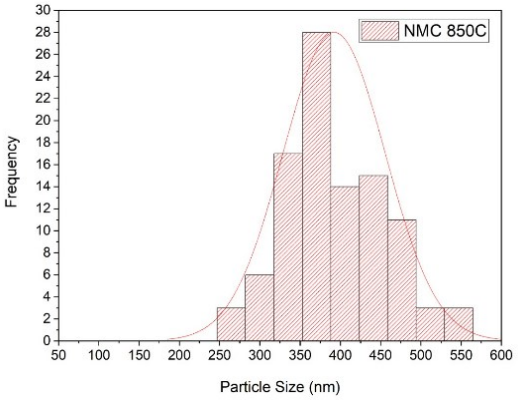

(d)

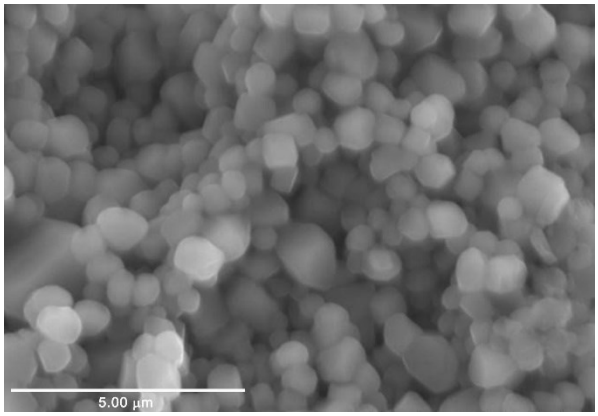

(e)

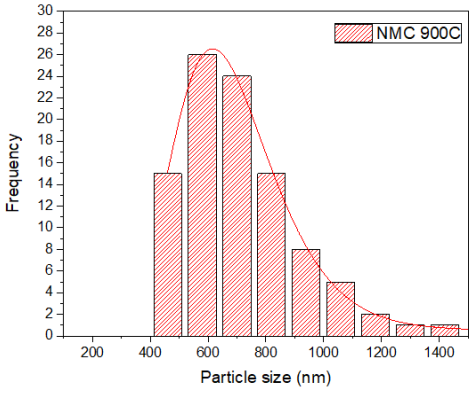

(f)

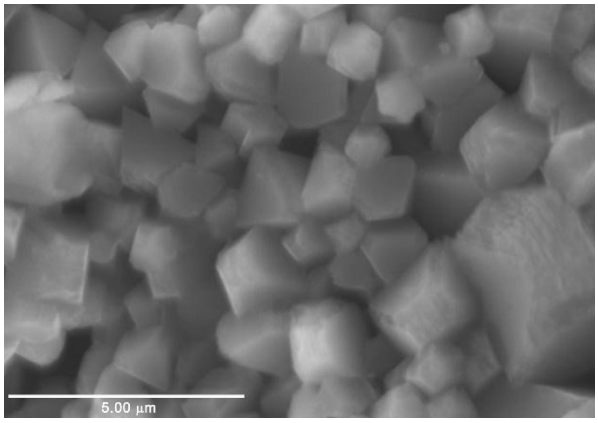

(g)

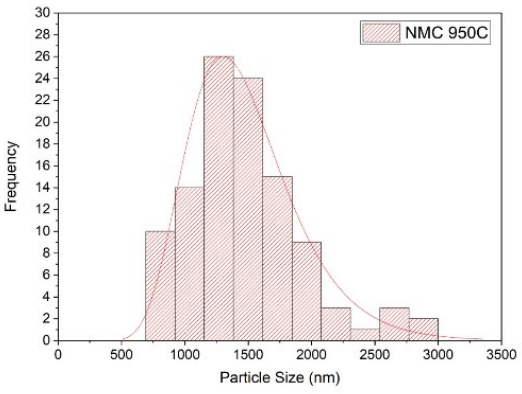

(h)

Fig. 5. SEM images of particles NMC111 synthesized by coprecipitation methods of (a) 800°C, (c) 850°C, (e) 900°C, (g) 950°C, and histogram images of particles NMC111 using imageJ program (b) 800°C, (d) 850°C, (f) 900°C, (h) 950°C.

SEM-EDS mapping results shown in Fig. 6 exhibit a relatively even distribution of Ni, Mn, and Co on each grain. This confirms the homogeneity of cathode powders composition regardless of calcination temperature. Homogeneous powders are the desired outcomes from the synthesis process, as the quality and durability of the cathode are heavily reliant to the powders' uniformity.

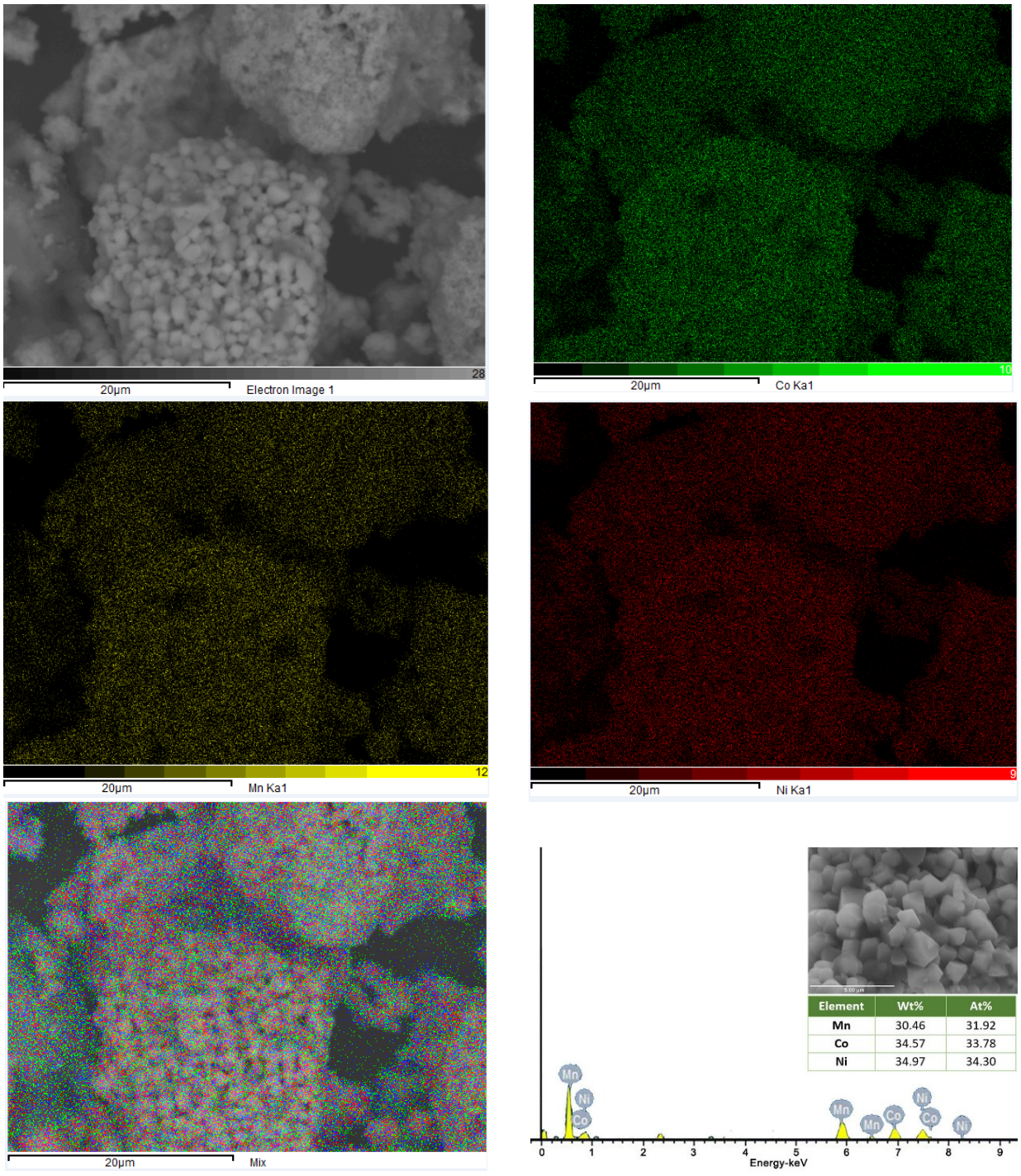

Fig. 6 EDS mapping of NMC111 800°C.

Particle size distribution of cathode powders using PSA is represented in Table 3. The average particle sizes analyzed with PSA at temperature variations of 800°C and 850°C display relatively similar results compared to SEM calculations, in which D50 values from PSA are 274.4 and 339.6 nm, respectively, and average particle size from SEM are 300 and 350 nm, respectively. According to SEM and PSA analysis, temperature variation of 800°C demonstrates the most homogeneous particle size compared to other temperature variations. Meanwhile, on a temperature variation of 900°C, the average particle size value analyzed with SEM is relatively higher than PSA, which can be the result of

sample preparation prior to PSA test. PSA test preparation involves mechanical procedures, which include dispersing the powders in liquid and placing it inside ultrasonic homogenizer. During mechanical preparation, powders can collide and crash into each other, which can reduce their overall particle sizes [21]. While in SEM, this preceding mechanical process is not required, and it only captures a small area of the powders, thus the particle size analysis results may differ. On temperature variation of 950°C, average particle size from SEM analysis is spiking up to 1,250 nm, while its D50 value from PSA drops to 357.9 nm. Karunawan *et al.* [22] in their study mentioned that particle size is more likely to enlarge with calcination temperature elevation, thus temperature variation of 950°C is having the highest particle size value according to SEM analysis.

This phenomenon transpires due to a diffusion mechanism, which naturally occurs by heating up the powders at high temperature, which can cause crystal growth [23]. Yet the D50 from PSA analysis is decreasing on account of the previously explained mechanical preparation prior to PSA test. And it can be seen from Table 3 that the particle size ranges from temperature variation of 950°C is very wide compared to other temperature variations, which strengthen the possibility of the powders bumping into each other during homogenization process, which can reduce particle size, while still leaving some initial large powders intact.

Table 3. PSA analysis of NMC111 at different calcination temperatures.

Temperature	D10 (nm)	D50 (nm)	D90 (nm)
800 °C	226.7	274.4	330.1
850 °C	270.0	339.6	426.7
900 °C	388.2	486.1	619.7
950 °C	206.2	357.9	610.9

CONCLUSION

NMC111 particles of varying temperatures calcination has been successfully synthesized using coprecipitation. The XRD characterization shows single phase rhombohedral with space group $R\bar{3}m$. The clear splitting peaks at (006)/(012) and (018)/(110) indicate the materials are well-ordered and layered hexagonal structures. Moreover, the increasing temperature calcination of NMC111 shows an increase in the degree of crystallinity and crystallite sizes and lowers the intensity ratio. Calcination temperatures between 800°C and 850°C have fine crystallite size and no undesirable Li/Ni cationic mixing in the structure. While SEM observed the particle morphologies, calcination temperature lower than 900°C shows uniform rectangle or pyramid shape submicron particles. Meanwhile, calcination temperature at 950°C exhibits a submicron until micron rectangle or pyramid shape. The SEM-EDS mapping shows the homogeneity composition for all samples. The particle size distribution of cathode powders was observed to enlarge with calcination temperature elevation. Suggesting the lower calcination temperature will give potential material for a cathode of lithium-ion batteries.

ACKNOWLEDGMENT

This work was financially supported by the National Research and Innovation Agency; *"Rumah Program Teknologi Kendaraan Listrik Berbasis Baterai Berlisensi Indonesia*, year 2022."

AUTHOR CONTRIBUTION

S.R, A.U.S., R.T, and W.T.U equally contributed as the main contributors of this paper i.e., conceptualization, material preparation, formal analysis, and writing original draft. All authors read and approved the final version of the paper.

REFERENCES

[1] T. Kim, W. Song, D. -Y. Son, et al. H. Dong and G. M. Koenig, " Lithium-ion batteries: outlook on present, future, and hybridized technologies," " J. Mater. Chem. A, 7(7), 2942-2946, 2019, doi: https://doi.org/10.1039/C8TA10513H

[2] S. W. D. Gourley, T. Or, and Z.Chen, "Breaking Free from Cobalt Reliance in Lithium-Ion Batteries." iScience 23, 101505, 2020, doi:10.1016/j.isci.2020.101505 .

[3] H. Widiyandari, A. N. Sukmawati, H. Sutanto, et al, "Synthesis of LiNi0.8Mn0.1Co0.1O2 cathode material by hydrothermal method for high energy density lithium-ion battery," J. Phys. 1153, 012074, 2019, doi: 10.1088/1742-6596/1153/1/012074

[4] S. S. Nisa, M. Rahmawati, C. S. Yudha, et al, "A fast approach to obtain layered transition-metal cathode material for rechargeable batteries," Batteries, 8(1), 4, 2022doi//doi.org/10.3390/batteries80100 04

[5] X. Liu, K. Li, and X. Li, "The electrochemical performance and applications of several popular lithium-ion batteries for electric vehicles - A review," in Communications in computer and

information science", Springer Singapore, Singapore, 2018, p. 201–213.

[6] D. Peralta, J. Salomon, J.-F. Colin, et al, "Submicronic LiNi1/3Mn1/3Co1/3O2 synthesized by co-precipitation for lithium-ion batteries - Tailoring a classic process for enhanced energy and power density," J. Power Sources, 396, 527–532, 2018, doi: https://doi.org/10.1016/j.jpowsour.2018.06.075

[7] M. Malik, Ka Ho. Chan, G. Azimi, "Review on the synthesis of LiNixMnyCo1-x-yO2 (NMC) cathodes for lithium-ion batteries", Mater. Today Energy, 28, 2022, doi: 10.1016/j.mtener.2022.101066

[8] M. Li and J. Lu, "Cobalt in lithium-ion batteries," Science, 367, 6481, 979–980, 2020, doi: 10.1126/science.aba9168

[9] C. Liao, F. Li, and J. Liu, "Challenges and modification strategies of ni-rich cathode materials operating at high-voltage," Nanomaterials, 12, 11, 1888, 2022, doi: doi.org/10.3390/nano12111888

[10] H. Dong and G. M. Koenig, "A review on synthesis and engineering of crystal precursors produced via coprecipitation for multicomponent lithium-ion battery cathode materials," CrystEngComm, 22(9), 1514–1530, 2020, doi: https://doi.org/10.1039/C9CE00679F

[11] J. Zhang, J. Qiao, K. Sun, et al, "Balancing particle properties for practical lithium-ion batteries ," Particuology, 61, 18-29, 2022, https://doi.org/10.1016/j.partic.2021.05.006

[12] Y. Wang, J. Roller, & R. Maric. (2018). Morphology-Controlled One-Step Synthesis of Nanostructured LiNi1/3Mn1/3Co1/3O2 Electrodes for Li-Ion Batteries. ACS Omega, 3(4), 3966–3973. https://doi.org/10.1021/acsomega.8b00380

[13] C. Deng, L. Liu, W. Zhou, et al, "Effect of synthesis condition on the structure and electrochemical properties of Li[Ni1/3Mn1/3Co1/3]O2 prepared by hydroxide co-precipitation method," Electrochimica Acta, 53(5), 2441–2447, 2008, doi: https://doi.org/10.1016/j.electacta.2007.10.025

[14] N. N. Sinha, "The effect of particle size on performance of cathode materials of Li-ion". Journal of the indian institute of science 89: 381–92, 2009, doi:

[15] S. C. Yin, Y. H. Rho, I. Swainson, et al, "X-ray/Neutron diffraction and electrochemical studies of lithium de/re-intercalation in Li1-xCo1/3Ni1/3Mn1/3O2(x=0→1)," Chem. Mater. 18(7), 1901–1910, 2006, doi: doi.org/10.1021/acsomega.8b00380

[16] X. Zhang, W. J. Jiang, A. Mauger, et al, "Minimization of the cation mixing in Li1+x(NMC)1−xO2 as cathode material," J. Power Sources, 195(5), 1292–1301, 2010, doi: https://doi.org/10.1016/j.jpowsour. 2009.09. 029

[17] J. Zheng, P. Yan, L. Estevez, et al, "Effect of calcination temperature on the electrochemical properties of nickel-rich LiNi0.76Mn0.14Co0.10O2 cathodes for lithium-ion batteries," Nano Energy, 49, 538–548, 2018, doi: https://doi.org/10.1016/j.nanoen. 2018.04.077

[18] S. Engün, K. B. Dermenci, and S. Turan, "Mixed hydroxide precipitate-derived Li(Ni 0. 333 Co 0.333 Mn 0.333) O 2 as a cathode material for Li-Ion batteries," Int. J. Energy Res. 2022. doi: https://doi.org/10.1002/er.8751

[19] D. Commandeur, C. Sabado, T. E. Ashton, and J. A. Darr, "Combinatorial performance mapping of near-nmc111 li-ion cathodes," J. Materiomics 2021. Doi: https://doi.org/10.1016/j.jmat.2021.07.00

[20] Z. Shen, Y. Hu, R. Chen, X. He, K. Wu, Z. Cheng, P. Pan, L. Jiang, J. Mao, and C. Ni, "Excimer ultraviolet-irradiated exfoliated graphite loaded with carbon-coated SnOx small nanoparticles as advanced anodes for high-rate-capacity lithium-ion batteries," Nanoscale 11(16), 7744–7753 (2019). Doi: https://doi.org/10.1039/C8NR10379H

[21] K. J. Griffith, K. M. Wiaderek, G. Cibin, L. E. Marbella, and C. P. Grey, "Niobium tungsten oxides for high-rate lithium-ion energy storage," Nature 559(7715), 556–563 (2018). Doi: https://doi.org/10.1038/s41586-018-0347-0

[22] J. Karunawan, O. Floweri, S. P. Santosa, A. Sumboja, and F. Iskandar, "Stable layered-layered-spinel structure of the Li1.2Ni0.13Co0.13Mn0.54O2 cathode synthesized by ball-milling assisted solid-state method," J. Electroanal. Chem. 907, 116050 (2022). Doi: https://doi.org/10.1016/j.jelechem.2022.116050

[23] J. Zhu, T. Vo, D. Li, R. Lu, N. M. Kinsinger, L. Xiong, Y. Yan, and D. Kisailus, "Crystal growth of Li[Ni1/3Co1/3Mn1/3]O2 as a cathode material for high-performance lithium ion batteries," Cryst. Growth & Des. 12(3), 1118–1123 (2012). Doi: 10.1021/cg200565n